Peak Power Estimation of Vanadium Redox Flow Batteries Based on Receding Horizon Control

Citation for the original published paper (version of record):
Xiong, B., Dong, S., Li, Y. et al (2023). Peak Power Estimation of Vanadium Redox Flow Batteries Based on Receding Horizon Control. IEEE Journal of Emerging and Selected Topics in Power Electronics, 11(1): 154-165. http://dx.doi.org/10.1109/JESTPE.2022.3152588

(article starts on next page)

Peak Power Estimation of Vanadium Redox Flow Batteries Based on Receding Horizon Control

Binyu Xiong, *Member, IEEE*, Sidi Dong, Yang Li, *Member, IEEE,* Jinrui Tang, *Member, IEEE,* Zhongbao Wei, *Senior Member, IEEE,* and Yixin Su

***Abstract*—The peak power of vanadium redox flow batteries (VRBs) reflects the continuous charging and discharging power capability. Accurate estimation of peak power is essential for the safe, reliable, and efficient operation of VRB systems, but also challenging as it is limited by several factors such as currents, flow rates, temperature, and state of charge. This paper proposes an online model-based peak power estimation scheme for VRBs. First, the model parameters and states are accurately estimated using the recursive least squares with forgetting and the unscented Kalman filter, respectively. Next, based on a linear time-varying VRB model and the estimated states, the peak power prediction problem is formulated into an optimal control problem and solved online using receding horizon control (RHC). The influence of the predictive horizon on the estimated peak power is discussed. Finally, the effectiveness of the proposed RHC-based peak power estimation scheme is verified experimentally on a 5-kW/3-kWh VRB platform.**

***Index Terms*—vanadium redox flow battery, online estimation, peak power estimation, receding horizon control, state of charge.**

I. Introduction

Vanadium redox flow batteries (VRBs) have great potential for large-scale energy storage systems (ESSs) due to their high degree of safety, long cycle life, high overload capability, and considerable flexibility in independently selecting the power and energy capacities [1]–[4]. Such a large-scale VRB-ESS can be used to effectively mitigate the impacts of variable and intermittent renewable powers on electricity grid systems. Conventionally, the VRBs have been designed for applications with very long-term operations where the delivered power is relatively low and less varying. However, modern power systems require the ESSs to actively participate in the grid regulation, such as to provide fast frequency response in a very short time frame. In this situation, the power capability of the ESSs shall play a critical role in maximizing the benefits both for the gencos and the system operators. Such a capability is usually signified by the peak power, defined as the maximum power that can be continuously delivered or absorbed over a specified period of time and within a safe operating area (SOA) [5]–[8]. The peak power can provide some basic information for scheduling and power flow control while ensuring system safety.

Unfortunately, the actual peak power of VRBs is neither provided in system specifications nor directly measurable. Thus, the next-generation battery management systems (BMS) for the VRB-ESSs should be able to monitor the peak power capability accurately. Although the peak power estimation has been extensively investigated in the literature, most relevant works focus on more widely deployed lithium-ion batteries [9]. These methods can be divided into two major categories, i.e., the methods based on a static characteristic map (CM) and the methods based on a dynamic model.

A CM method utilizes massive experimental data measured under different temperatures, state of charge (SOC), and time scales. The experimental data are usually obtained offline with the hybrid pulse power characteristic (HPPC) test method [10]. However, such a method has several disadvantages. First, it only considers the operating constraint on terminal voltage, resulting in inaccurate peak power estimation. Second, since the dynamic behaviors of the batteries are ignored in the HPPC test, the CM method cannot be used to estimate the peak power of the battery under practical operating conditions. Furthermore, this method can only estimate the instantaneous peak power, that is, the permissible power at the current time instant, but cannot be used to estimate a continuous peak power that the battery can provide within a long time horizon, which is usually required for power system planning and operation [10].

In contrast, the peak power estimation methods based on equivalent circuit models (ECMs) are more adaptable and robust by taking into account the constraints on current, voltage, SOC, as well as time-varying model parameters [11], [12]. However, the effectiveness of these methods depends heavily on the accuracy of the estimated SOC, model parameters, and peak power prediction algorithm, which poses two main challenges for VRBs. First, the SOC is determined by the concentration of vanadium ions in the stack [13], which cannot be measured directly. Second, the model parameters of VRBs are affected by the current, temperature, flow rate, SOC, amongst other factors, usually in a highly nonlinear and time-varying manner [14]. Therefore, SOC estimation and parameter identification algorithms lay the foundation for reliable ECM-based peak power estimation for VRBs.

Existing SOC estimation methods can be divided into three categories [15]: 1) Direct measurement methods; 2) Data-driven estimation methods; 3) Model-based estimation methods.

This work was supported in part by the National Natural Science Foundation of China under Grant 61703318.

Binyu Xiong, Sidi Dong, Jinrui Tang, and Yixin Su are with the School of Automation, Wuhan University of Technology, Wuhan, 430070, China (e-mail: bxiong2@whut.edu.cn; sididong@whut.edu.cn; tangjinrui@whut.edu.cn; suyixin@whut.edu.cn).

Yang Li is with the School of Automation, Wuhan University of Technology, Wuhan, 430070, China, and also with the Department of Electrical Engineering, Chalmers University of Technology, Gothenburg, 41296, Sweden (e-mail: yangli@ieee.org).

Zhongbao Wei is with the National Engineering Laboratory for Electric Vehicles, Beijing Institute of Technology, Beijing 100081, China (e-mail: weizb@bit.edu.cn).

The direct measurement methods include the Coulombic counting and the open-circuit voltage (OCV) methods. The Coulombic counting method uses the applied current for time integration. This technique is straightforward, but the performance is subject to the accuracy of the current sensor, Coulombic efficiency, and initial SOC. The OCV method applied the measured OCV and the OCV−SOC relationship to estimate the SOC. For VRBs, the performance of the direct measurement method is poor, and thus it is rarely used [15]. The data-driven methods adopt neural networks [16], fuzzy logic [17], or support vector machines [18]. For example, Weigert *et al.* [16] proposed a backpropagation neural network for the VRB SOC estimation. Mellado *et al*. [17] used a fuzzy battery model for an online SOC estimation method. Although simple to design and implement, the data-driven methods require massive data for model training and validation, which may not be available for practical systems. Besides, the computational costs of these methods are high, and thus it is not desirable to use such a method for low-cost implementation. The model-based methods include the sliding mode observer (SMO) [19], the extended Kalman filter (EKF) [20], and the unscented Kalman filter (UKF) [21], and they have shown an excellent balance between computational efficiency and predictive accuracy. For instance, Xiong *et al*. [19] designed an SMO to estimate the SOC and capacity of VRBs jointly. Qiu *et al*. [20] proposed an EKF-based SOC estimator based on a dynamic electrical model of VRBs. However, the linearization error of the EKF-based method leads to low accuracy, and the algorithm is computationally inefficient since it needs to calculate the Jacobian matrix sequentially. To solve the problems of the EKF, Zheng *et al*. [21] proposed the UKF to estimate SOC. Unfortunately, the time-varying parameters of these models have not been considered for practical applications, which can lead to significant estimation error.

Also, many works study parameter identification for VRBs [22]-[25]. For example, Qiu *et al*. [22] proposed a simplified VRB equivalent model for the integration with wind energy systems. In their work, the model parameters were identified with empirical equations, whereas experimental validation is lacking. In [23], Zhang *et al*. developed a comprehensive ECM of VRBs considering the influence of self-discharge and pump power losses. The authors also analyzed the model parameters under various current and flow rates. Later, Xiong *et al*. [24] proposed an improved VRB electro-thermal model and used particle swarm optimization to identify the model parameters offline. However, the offline methods require time-consuming off-grid experiments that can interrupt the operation of the system in practice. Furthermore, since the parameters of VRBs are affected by many factors, high-dimensional look-up tables are needed to cover the entire operating regimes, increasing the computational burden significantly. Hence, online methods have received growing research attention in recent years. For example, Mohamed *et al*. [25] proposed a second-order resistor-capacitor (RC) model for VRBs and used the EKF to identify the model parameters online. However, the computational burden for generating the Jacobian and performing matrix inversion in the EKF is heavy for a seventh-order battery model. The least-squares (LS) method can be used to avoid this problem, exhibiting its excellence for online parameters identification [26]. However, the OCV of the battery needs to be captured offline in the parameter identification methods mentioned above. A recursive LS method (RLS) was thus proposed in [27] for online parameter identification where the OCV is measured under low current conditions. Nevertheless, the OCV cannot be accurately measured under high power conditions due to the large voltage drop in the stack and the presence of measurement noises.

Accurate estimation of peak power is also affected by the prediction algorithm for peak power. Feng *et al*. [28] proposed a peak power prediction method in which the OCV is considered constant over a short time horizon. However, as the time horizon increases, the OCV can change significantly, especially under high power conditions. Yang *et al*. [26] solved this problem by considering the dependence of the OCV on SOC and obtained improved peak power prediction over a long period. However, this method only considers the limits of the terminal voltage and current. It should be noted that the SOC can also affect the peak power, especially at very high or very low SOC regions [29]. Wei *et al*. [27] thus proposed a peak power estimation algorithm considering the constraints on current, terminal voltage, and SOC. This algorithm has the same structure as the peak power estimation algorithm adopted in [5]-[7], [30], where the current in the estimation period was assumed constant. The peak power estimation is further simplified to the peak current estimation due to the strict correlation between the terminal voltage and the current. However, this method can cause considerable estimation error at the high and low SOC regions. In addition, the maximum allowable currents are highly dynamic due to the rapidly changed terminal voltage, and there is also a highly nonlinear relationship between the peak power and the peak current.

Hence, although the model-based peak power estimation methods are promising for VRBs, they still present two challenges. First, the SOC cannot be accurately estimated due to time-varying model parameters. Second, the peak power can vary significantly with increased prediction horizons and more dynamic operation conditions. To this end, this paper proposes a new peak power estimation scheme to address the above research problems. The method is based on an experimentally verified ECM of the VRBs, where the model parameters are identified based on a combination of offline tests and the online recursive least squares with forgetting (FRLS), and the UKF is adopted to estimate the states of VRBs. With the verified high accuracy in estimated battery states and parameters, as the major contribution of the present investigation, we next formulate the peak power prediction as a finite time-horizon optimal control problem, and the problem was solved using the receding horizon control (RHC). Specifically, by rewriting the developed nonlinear VRB model as a linear time-varying (LTV) form and considering the constraints on current, voltage, and SOC, the optimization problem is updated and solved repeatedly online using the quadratic programming, achieving accurate and low-cost peak power estimation.

II. Modeling and SOC Estimation of VRBs

A. Vanadium Redox Flow Battery Model

To capture the complex characteristics of VRBs during operation, an accurate model of VRBs needs to be established first. Among various existing VRB modeling methods, the first-order RC ECM has shown high accuracy under a wide range of operating conditions with a simple model structure. As shown in Fig. 1, such an ECM consists of four components, including 1) a voltage source E_{ocv}, representing the OCV and it is affected by the concentrations of various vanadium species and protons; 2) a resistance R_{shunt}, connected in parallel with E_{ocv}, and it is used to describe the self-discharge phenomenon due to the movement of vanadium ions through the conduits and channels; 3) a series-connected R_0, representing the ohmic loss due to the resistances in the electrodes, electrolyte, and membrane; and 4) a parallel RC pair consisting of a polarization resistance R_1 and a polarization capacitance C_1, which is used for emulating the dynamic behavior due to ion diffusion. The ion diffusion results in the concentration gradient between the bulk electrolyte and the electrode surface, which causes the concentration overpotential as a consequence. The ECM in Fig. 1 is described by,

$$\frac{d\text{SOC}(t)}{dt} = \frac{\eta I(t)}{C_N} \tag{1}$$

$$\frac{dU_1(t)}{dt} = -\frac{U_1(t)}{R_1C_1} + \frac{I(t)}{C_1} \tag{2}$$

$$U_t(t) = E_{\text{ocv}}(t) - U_1(t) - R_0 I(t) \tag{3}$$

where I is the applied current, U_t is the terminal voltage, U_1 is the voltage across the RC pair, and C_N is the nominal capacity of the VRB. In (3), the OCV is a nonlinear function $f_{\text{ocv}}(\cdot)$ of SOC, i.e.,

$$E_{\text{ocv}} = f_{\text{ocv}}(\text{SOC}) = E^{\Theta} + m\frac{2R_gT_S}{\zeta F}[k_1\ln(\text{SOC}) - k_2\ln(1-\text{SOC})] \tag{4}$$

where E^{Θ}, R_g, F, ζ, and m are the formal potential of the VRB, the universal gas constant, Faraday's constant, the number of electrons transferred, and the number of cells in the stack, respectively. k_1 and k_2 are two correction coefficients. T_S is the electrolyte temperature in the stack, considered as a constant (T_S = 298.15 K) in this work. In addition, η is the Coulombic efficiency, defined by

$$\eta = 1 - \frac{E_{\text{ocv}}}{R_{\text{shunt}}I} \tag{5}$$

B. Parameter Identification

Accurate model parameters are essential for reliable peak power estimation. Considering the time scale for peak power estimation, the parameters in the model presented in Section II-A can be divided into two groups. First, the capacity C_N, shunt resistance R_{shunt}, and parameters in (4) do not change rapidly, and thus they can be considered constant and identified offline [24]. On the other hand, the circuit parameters R_0, R_1, and C_1 are usually significantly affected by temperature, SOC, current, electrolyte flow rate, etc., and thus, they need to be identified

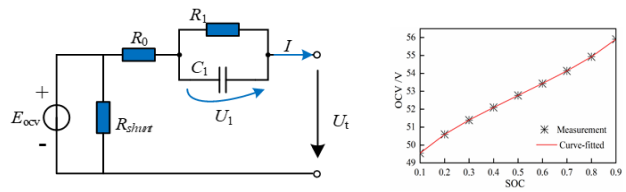

(a) (b)

Fig. 1. A first-order RC ECM of VRBs: (a) schematic of first-order RC model considering self-discharge and (b) measured and fitted SOC–OCV relationship of $E_{\text{ocv}} = f_{\text{ocv}}(\text{SOC})$.

online based on measured data. As mentioned earlier, the RLS method demonstrates the excellent capability for online parameters identification due to low requirements on computation. In this method, (2) and (3) are first discretized with the sampling time T using the bilinear transform, i.e.,

$$U_{t,k} = \hat{\theta}_k^{\top}\varphi_k \tag{6}$$

where

$$\varphi_k = \begin{bmatrix} E_{\text{ocv},k} & U_{t,k-1} & I_k & I_{k-1} \end{bmatrix}^{\top} \tag{7}$$

$$\hat{\theta}_k = [1-a_3 \quad a_3 \quad a_1 \quad a_2]^{\text{T}} \tag{8}$$

Here, the subscript $k = t/T$ is the discrete-time instant, and the superscripted "$\top$" represents transpose. The coefficients a_1, a_2, and a_3 are functions of circuit parameters and the sampling time:

$$\begin{cases} a_1 = \dfrac{R_0T + R_1T + 2R_0R_1C_1}{T + 2R_1C_1} \\ a_2 = \dfrac{R_0T + R_1T - 2R_0R_1C_1}{T + 2R_1C_1} \\ a_3 = \dfrac{T - 2R_1C_1}{T + 2R_1C_1} \end{cases} \tag{9}$$

However, the accuracy of the RLS would drop dramatically due to data saturation. A forgetting factor λ_θ can thus be introduced into the RLS. As a result, smaller weights will be assigned to the previous data [5]. The model parameters can be updated with new information from measurements. Such an FRLS method is thus employed in this work to identify the time-varying R_0, R_1, and C_1. The procedures for updating the parameter vector θ_k based on the FRLS algorithm are given in Table I. After θ_k is obtained, the circuit parameters can be calculated by:

TABLE I
FRLS-BASED ONLINE VRB PARAMETER IDENTIFICATION

1. Initialization:

$$\hat{\theta}_0^{+} = \text{E}[\theta_0],\ \ P_{\theta,0}^{+} = \text{E}[(\theta_0 - \hat{\theta}_0)(\theta_0 - \hat{\theta}_0)^{\top}]$$

where E[·] represents the expected value and the hat "^" represents the estimated value.

2. Prior (denoted by "+") parameter and covariance matrix update:

$$\hat{\theta}_k^{-} = \hat{\theta}_{k-1}^{+} \quad P_{\theta,k}^{-} = P_{\theta,k-1}^{+} \tag{11}$$

3. Gain update:

$$L_{\theta,k} = P_{\theta,k}^{-}\varphi_k(\lambda_\theta + \varphi_k^{\top}P_{\theta,k}^{-}\varphi_k)^{-1} \tag{12}$$

4. Posterior (denoted by "–") parameter and covariance matrix update:

$$\hat{\theta}_k^{+} = \hat{\theta}_k^{-} + L_{\theta,k}[U_{t,k} - (\hat{\theta}_k^{-})^{\top}\varphi_k] \tag{13}$$

$$P_{\theta,k}^{+} = (I_4 - L_{\theta,k}\varphi_k^{\top})P_{\theta,k}^{-}\lambda_\theta^{-1} \tag{14}$$

where I_4 is a 4×4 identity matrix, and λ_θ is set to 0.97 as an initial value.

TABLE II
UKF-BASED VRB STATE ESTIMATION

1. Initialize UKF state, covariance, and measurement noise, and model:

$$\hat{x}_0^+ = \mathrm{E}(x_0)\ ,\ P_0^+ = \mathrm{E}[(x_0 - \hat{x}_0^+)(x_0 - \hat{x}_0^+)^\top]$$

2. Generate $2n + 1$ sigma points:

$$x_{k-1}^i = \begin{cases} \hat{x}_{k-1}^+ & i = 0 \\ \hat{x}_{k-1}^+ + (\sqrt{(n+\lambda)P_{k-1}^+})_i & 1 \le i \le n \\ \hat{x}_{k-1}^+ - (\sqrt{(n+\lambda)P_{k-1}^+})_i & n+1 \le i \le 2n \end{cases} \tag{15}$$

where λ represents a scaling parameter and $n = 2$ is the model order.

3. Update the prior state estimates of the $2n + 1$ sigma points:

$$\hat{x}_k^i = F(\hat{x}_{k-1}^i, u_k) + w_k \tag{16}$$

where $F(\cdot)$ represents the discretized state transition equation based on (1) and (2). $w_k \sim \mathcal{N}(0, \mathcal{Q})$ represents the process uncertainty with zero mean and the covariance of $\mathcal{Q}$.

4. Compute the mean and covariance of state vector:

$$\hat{x}_k^- = \sum_{i=0}^{2n} w_m^i \hat{x}_k^i \tag{17}$$

$$P_k^- = \sum_{i=0}^{2n} w_c^i (x_k^i - \hat{x}_k^-)(x_k^i - \hat{x}_k^-)^\top + \mathcal{Q} \tag{18}$$

where w_m^i and w_c^i are weighting factors.

5. Update the terminal voltage

$$\begin{cases} \hat{U}_{t,k}^i = H(\hat{x}_k^i, u_k) + v_k \\ \hat{U}_{t,k}^- = \sum_{i=0}^{2n} w_m^i \hat{U}_{t,k}^i \end{cases} \tag{19}$$

where $H(\cdot)$ represents the output equation (3). $v_k \sim \mathcal{N}(0, \mathcal{R})$ represents the measurement noise with zero mean and covariance of $\mathcal{R}$.

6. Calculate the measurement covariance and cross-covariance of state and measurement

$$\begin{cases} P_{xy,k} = \sum_{i=0}^{2n} w_c^i (\hat{x}_k^i - \hat{x}_k^-)(\hat{U}_{t,k}^i - \hat{U}_{t,k}^-)^\top \\ P_{yy,k} = \sum_{i=0}^{2n} w_c^i (\hat{U}_{t,k}^i - \hat{U}_{t,k}^-)(\hat{U}_{t,k}^i - \hat{U}_{t,k}^-)^\top + \mathcal{R} \end{cases} \tag{20}$$

7. Calculate the Kalman gain, the posterior state variables, and the posterior state covariance matrix.

$$\begin{cases} K_k = P_{xy,k} P_{yy,k}^{-1} \\ \hat{x}_k^+ = \hat{x}_k^- + K_k (U_{t,k} - \hat{U}_{t,k}^-) \\ P_k^+ = P_k^- - K_k P_{yy,k} K_k^\top \end{cases} \tag{21}$$

$$\begin{bmatrix} R_0 & R_1 & C_1 \end{bmatrix} = \begin{bmatrix} \dfrac{a_2 - a_1}{1 + a_3} & \dfrac{2(a_2 + a_3 a_1)}{a_3^2 - 1} & \dfrac{-(a_3+1)^2}{4(a_2 + a_3 a_1)} \end{bmatrix} \tag{10}$$

C. State Estimation

In the first-order RC ECM as presented in Section II-A, the state variables include the SOC and the polarization voltage U_1, denoted by the state vector $x = [\mathrm{SOC}, U_1]^\top$. Since the states are not measurable, a state estimator is needed by using the developed model and incorporating the information from voltage measurement $y = U_t$. Among numerous state estimation methods, the UKF-based state estimator uses a statistical method based on the unscented transform to avoid the linearization errors in the EKF. As the UKF exhibits better performance on state estimation for nonlinear systems [31], [32], it is adopted in this paper to achieve high accuracy in state estimation, and the algorithm is described in Table II. Along with the FRLS-based parameter identification method, the FRLS-UKF co-estimation method can be used to jointly monitor the time-varying parameters and states online, and these estimates serve as core information for the peak power estimation in the following section.

III. RHC-BASED PEAK POWER ESTIMATION

In this work, an RHC-based method is proposed to predict the VRB peak power. RHC, also known as model predictive control, is a widely used control strategy where the control action is optimally determined by predicting the future behaviors of the system with the capability to consider operating constraints [33]. The design procedure of the RHC-based peak power prediction method is described in this section.

A. Predictive Model

First, the OCV can be calculated recursively by using the first-order Taylor series polynomial to approximate the OCV vs. SOC relationship, i.e. [33],

$$E_{\mathrm{ocv},k+1} \approx E_{\mathrm{ocv},k} + f'_{\mathrm{ocv}}(\mathrm{SOC}_k)(\mathrm{SOC}_{k+1} - \mathrm{SOC}_k) \tag{22}$$

where $f'_{\mathrm{ocv}}(\cdot)$ represents the derivative function of $f_{\mathrm{ocv}}(\cdot)$.

According to (1), the SOC can be expressed as,

$$\mathrm{SOC}_{k+1} = \mathrm{SOC}_k - \eta I_k T / C_N \tag{23}$$

Substituting (23) into (22), we have

$$E_{\mathrm{ocv},k+1} = E_{\mathrm{ocv},k} - (\eta T / C_N) f'(\mathrm{SOC}_k) I_k \tag{24}$$

Hence, the VRB model (1)–(3) presented in Section II-A can be discretized using the exponential integrator and augmented as an LTV state-space form

$$\chi_{k+1} = \underbrace{\begin{bmatrix} 1 & 0 & 0 \\ 0 & e^{-T/R_1C_1} & 0 \\ 0 & 0 & 1 \end{bmatrix}}_{\tilde{A}} \chi_k + \underbrace{\begin{bmatrix} -T/C_N \\ 1 - e^{-T/R_1C_1} \\ -f'_{\mathrm{ocv}}(\mathrm{SOC}_k)\eta T / C_N \end{bmatrix}}_{\tilde{B}} u_k \tag{25}$$

$$y_k = \underbrace{\begin{bmatrix} 0 & -1 & 1 \end{bmatrix}}_{\tilde{C}} \chi_k + \underbrace{(-R_0)}_{\tilde{D}} u_k \tag{26}$$

where $\chi = [\mathrm{SOC}, U_1, E_{\mathrm{ocv}}]^\top$ is the augmented state vector, $y_k = U_{t,k}$ is the voltage output, and $u_k = I_k$ is the single input. Equations (25) and (26) will be used next as the predictive model in a proposed RHC-based peak power estimator.

B. Constrained Optimization Problem for VRB Peak Power Estimation

The objective for peak power estimation is to calculate the maximum accumulated power over a future time horizon M. Such an estimation problem can be formulated into an optimal control problem, in which the control objective is to find an input sequence $\vec{u}^M = [I_{k+1}, \cdots, I_{k+M}]$ to achieve the maximum charging or discharging power.

Several factors limit the peak power of VRBs. First, the battery current is limited by the ratings of cables, fuses, power converters, etc. Here, we assume the current should be limited between $I_{\min}$ and $I_{\max}$. Note that $I_{\min}$ will be set the zero for calculating the discharging peaker power, while $I_{\max}$ shall be set to zero for the charging peal power. Next, to avoid overcharge and over-discharge, the VRB should also operate within safe ranges of SOC and voltage, denoted by [$\mathrm{SOC}_{\min}$, $\mathrm{SOC}_{\max}$] and [$U_{t,\min}$, $U_{t,\max}$], respectively. In this regard, a constrained optimization problem can be formulated at time instant k: Given

the model parameters and the estimated augmented state vector $\chi_k = \hat{\chi}_k$, find the current sequence $\vec{u}^{M*} = [I^*_{k+1}, \cdots I^*_{k+M}]$, so that

$$\max_{\vec{u}^M} J = \max_{\vec{u}^M} \sum_{i=1}^{M} \left(u_{k+i} y_{k+i} \right) \;\Rightarrow\; \min_{\vec{u}^M} \left(-\left| \sum_{i=1}^{M} u_{k+i} y_{k+i} \right| \right) \quad (27)$$

s.t. $\forall i \in \{1, 2, \cdots, M\}$

$$\begin{cases} \chi_{k+i} = \tilde{A}\chi_{k+i-1} + \tilde{B}u_{k+i-1} \\ y_{k+i} = \tilde{C}\chi_{k+i} + \tilde{D}u_{k+i} \end{cases} \quad (28)$$

$$\begin{cases} I_{\min} \le u_{k+i} \le I_{\max} \\ U_{t,\min} \le y_{k+i} \le U_{t,\max} \\ \mathrm{SOC}_{\min} \le z_{k+i} \le \mathrm{SOC}_{\max} \end{cases} \quad (29)$$

where J represents the cost of the objective function and z represents the SOC for brevity.

Since the predictive model (25) and (26) is linear time-varying, such a constrained optimization problem (27)−(29) can be transformed into a quadratic programming (QP) problem [33]. The procedure will be described as follows.

First, the predicted augmented state vectors over the prediction horizon M can be calculated sequentially as,

$$\begin{cases} \chi_{k+1} = \tilde{A}\chi_k + \tilde{B}u_k \\ \chi_{k+2} = \tilde{A}^2\chi_k + \tilde{A}\tilde{B}u_k + \tilde{B}u_{k+1} \\ \quad\vdots \\ \chi_{k+M} = \tilde{A}^M\chi_k + \sum_{j=0}^{M-1} \tilde{A}^{M-1-j}\tilde{B}u_{k+j} \end{cases} \quad (30)$$

which can be rewritten in a matrix form, i.e.,

$$\vec{\chi}^M = p\chi_k + Q\vec{u}^M \quad (31)$$

where

$$\vec{\chi}^M = \begin{bmatrix} \chi_{k+1} \\ \chi_{k+2} \\ \vdots \\ \chi_{k+M} \end{bmatrix}, \; p = \begin{bmatrix} \tilde{A} \\ \tilde{A}^2 \\ \vdots \\ \tilde{A}^M \end{bmatrix}, \; Q = \begin{bmatrix} \tilde{B} & 0 & \cdots & 0 \\ \tilde{A}\tilde{B} & \tilde{B} & \cdots & 0 \\ \vdots & \vdots & \ddots & 0 \\ \tilde{A}^{M-1}B & \tilde{A}^{M-2}\tilde{B} & \cdots & \tilde{B} \end{bmatrix}$$

The predicted terminal voltage vector over the prediction horizon M can also be obtained sequentially as,

$$\begin{cases} y_{k+1} = \tilde{C}\tilde{A}\chi_k + \tilde{C}\tilde{B}u_k + \tilde{D}u_{k+1} \\ y_{k+2} = \tilde{C}\tilde{A}^2\chi_k + \tilde{C}\tilde{A}\tilde{B}u_k + \tilde{C}\tilde{B}u_{k+1} + \tilde{D}u_{k+2} \\ \quad\vdots \\ y_{k+M} = \tilde{C}\tilde{A}^M\chi_k + \tilde{C}\tilde{A}^{M-1}\tilde{B}u_k + \cdots + \tilde{D}u_{k+M} \end{cases} \quad (32)$$

Similarly, (32) can be rewritten in matrix form as,

$$\vec{y}^M = f\chi_k + G\vec{u}^M \quad (33)$$

where

$$\vec{y}^M = \begin{bmatrix} y_{k+1} \\ y_{k+2} \\ y_{k+3} \\ \vdots \\ y_{k+M} \end{bmatrix}, f = \begin{bmatrix} \tilde{C}\tilde{A} \\ \tilde{C}\tilde{A}^2 \\ \tilde{C}\tilde{A}^3 \\ \vdots \\ \tilde{C}\tilde{A}^M \end{bmatrix}, G = \begin{bmatrix} \tilde{C}\tilde{B} & \tilde{D} & 0 & \cdots & 0 \\ \tilde{C}\tilde{A}B & \tilde{C}\tilde{B} & \tilde{D} & \cdots & 0 \\ \tilde{C}\tilde{A}^2\tilde{B} & \tilde{C}\tilde{A}\tilde{B} & \tilde{C}\tilde{B} & \cdots & 0 \\ \vdots & \vdots & \vdots & \ddots & \vdots \\ \tilde{C}\tilde{A}^{M-1}\tilde{B} & \tilde{C}\tilde{A}^{M-2}\tilde{B} & \tilde{C}\tilde{A}^{M-3}\tilde{B} & \cdots & \tilde{D} \end{bmatrix}$$

With (31) and (33), the objective function in (27) can be converted to

$$\begin{aligned} J &= -\left| \sum_{i=1}^{M} u_{k+i} y_{k+i} \right| = -\left| (\vec{u}^M)^\top \vec{y}^M \right| \\ &= -\left| \frac{1}{2} (\vec{u}^M)^\top \underbrace{(2G)}_{W} \vec{u}^M + \underbrace{(f\chi_k)^\top}_{V} \vec{u}^M \right| \end{aligned} \quad (34)$$

By combining (33) with the voltage constraint in (29), we obtain,

$$\begin{bmatrix} G \\ -G \end{bmatrix} \vec{u}^M \le \begin{bmatrix} \vec{y}^M_{\max} - f\chi_k \\ -(\vec{y}^M_{\min} - f\chi_k) \end{bmatrix} \quad (34)$$

where $\vec{y}^M_{\max} \in \mathbb{R}^M$ and $\vec{y}^M_{\min} \in \mathbb{R}^M$ contains the upper voltage limit $U_{t,\max}$ and the lower voltage limit $U_{t,\min}$, respectively.

Next, the SOC sequence $\vec{z}^M$ over the prediction horizon M can be expressed as,

$$\vec{z}^M = H(p\chi_k + Q\vec{u}^M) \quad (35)$$

where $H = \mathrm{diag}(\underbrace{[e_1, \quad e_1, \quad \cdots \quad e_1]}_{M})$ and $e_1 = [1 \;\; 0 \;\; 0]$,

By substituting (35) into the third inequality of (29), the constraint on SOC can be expressed as,

$$\begin{bmatrix} HQ \\ -HQ \end{bmatrix} \vec{u}^M \le \begin{bmatrix} \vec{z}^M_{\max} - Hpx_k \\ -(\vec{z}^M_{\min} - Hpx_k) \end{bmatrix} \quad (36)$$

where $\vec{z}^M_{\max} \in \mathbb{R}^M$ and $\vec{z}^M_{\min} \in \mathbb{R}^M$ contains the upper SOC limit $\mathrm{SOC}_{\max}$ and the lower SOC limit $\mathrm{SOC}_{\min}$, respectively.

Based on (34) and (36), the inequality constraints in (29) can be expressed as

$$\underbrace{\begin{bmatrix} L \\ -L \\ G \\ -G \\ Hq \\ -Hq \end{bmatrix}}_{A} \vec{u}^M \le \underbrace{\begin{bmatrix} \vec{u}^M_{\max} \\ -\vec{u}^M_{\min} \\ \vec{y}^M_{\max} - f\chi_k \\ -(\vec{y}^M_{\min} - f\chi_k) \\ \vec{z}^M_{\max} - HQ\chi_k \\ -(\vec{z}^M_{\min} - HQ\chi_k) \end{bmatrix}}_{b} \quad (37)$$

where L is M-dimensional identity matrix, and $\vec{u}^M_{\max} \in \mathbb{R}^M$ and $\vec{u}^M_{\min} \in \mathbb{R}^M$ are the upper and lower limits of sequential constraints for currents, respectively.

With the matrices W, V, A, and vector b in (34) and (37), one can consider the optimization problem as a standard QP problem and solve it with a well-developed QP solver. In this work, we use the function *quadprog* in MATLAB with the interior-reflective Newton method for solving this QP problem sequentially. Once the optimal current sequence $\vec{u}^{M*}$ is obtained, the VRB terminal voltage sequence $\vec{y}^{M*} = [U^*_{t,k+1}, \cdots U^*_{t,k+M}]$ can be estimated by (33). Multiplying $\vec{u}^{M*}$ by $\vec{y}^{M*}$ yields the peak power sequence, denoted by $\left[P^{\mathrm{dis}*}_{k+1}, P^{\mathrm{dis}*}_{k+2}, ..., P^{\mathrm{dis}*}_{k+M}\right]$ for discharging and $\left[P^{\mathrm{chg}*}_{k+1}, P^{\mathrm{chg}*}_{k+2}, ..., P^{\mathrm{chg}*}_{k+M}\right]$ for charging. The instantaneous peak power at time instant k is calculated by,

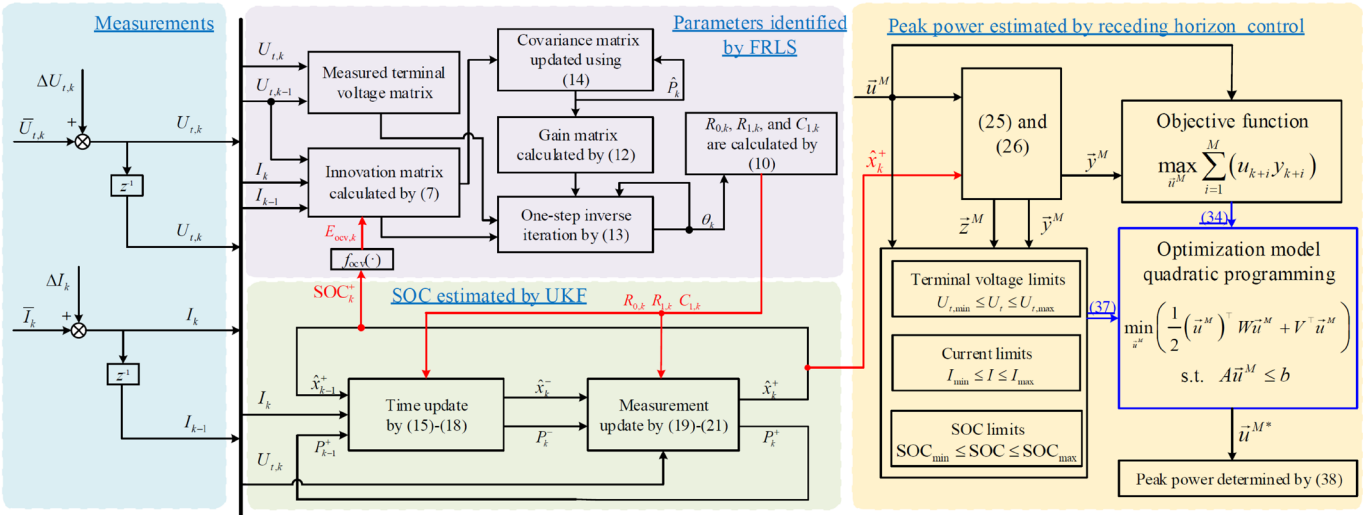

Fig. 2. Framework of proposed online peak power estimation scheme for VRBs.

$$\begin{cases} P_{\text{peak},k}^{\text{dis}} = \min(P_{k+1}^{\text{dis}*}, P_{k+2}^{\text{dis}*}, \ldots, P_{k+M}^{\text{dis}*}) \\ P_{\text{peak},k}^{\text{chg}} = \max(P_{k+1}^{\text{chg}*}, P_{k+2}^{\text{chg}*}, \ldots, P_{k+M}^{\text{chg}*}) \end{cases} \tag{38}$$

C. Summary of Proposed Online VRB Peak Power Estimation Scheme

The framework of the proposed online estimation scheme of VRB peak power is presented in Fig. 2. The main steps are summarized as follows:

Step 1: Data Collection. The currents and voltages are measured.

Step 2: Model Parameter Identification. Model parameters are updated using the measured voltage and current data according to the FRLS algorithm presented in Section II-A. Here, the OCV can be updated with (4) based on the prior estimate of the SOC, and the identified parameters (R_0, R_1, and C_1) will be used in the SOC and peak power estimators.

Step 3: State Estimation. With the updated model parameters R_0, R_1, and C_1, the UKF-based state estimator adjusts the prior state estimate of SOC and U_1 to minimize the voltage error. The posterior state estimate will be used for the peak power estimation.

Step 4: Peak Power Estimation. With the identified model parameters and estimated states, the optimal current sequence is obtained by solving the optimal control problem (27)−(29) based on the RHC (34) and (37). The peak power is finally obtained using (38).

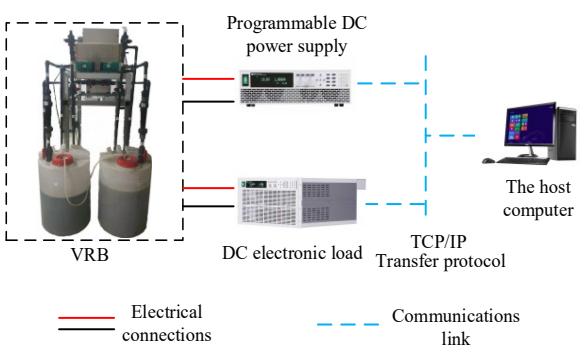

Fig. 3. Schematic of the VRB experimental setup.

IV. Experimental Setup and Design

A. Experimental Setup

To verify the proposed VRB peak power estimation scheme, a 5-kW/3-kWh VRB experimental platform was used, and a schematic diagram of the experimental setup is shown in Fig. 3. The platform includes a programmable dc power supply ITECH 6533C, a programmable dc electronic load ITECH 8818, a host computer, and a VRB. The VRB stack consists of 37 series-connected cells, and the nominal charge/discharge current is 100 A. The nominal voltage of VRB is 50 V at SOC = 0.5. The lower and upper voltage limits are 40 V and 60 V, respectively. The host computer is used to control the power flow and monitor the system conditions of the power supply, the electronic load, and the VRB. The host computer is also used for data storage, processing, and visualization. The specifications of the experimental platform are given in Table III.

Table III
Specifications of the VRB Experimental Platform

Configuration	Dimension
Power rating	5 kW
Capacity	3 kWh
Number of cells	37
Stack dimension	750 mm×480 mm×300 mm
Electrolyte volume	200 L
Concentration of vanadium ions	1.5 mol/L
Voltage lower/upper limits	40 V/60 V
Maximum discharge current	100 A
Maximum charge current	−100 A
SOC lower/upper limits	0/1

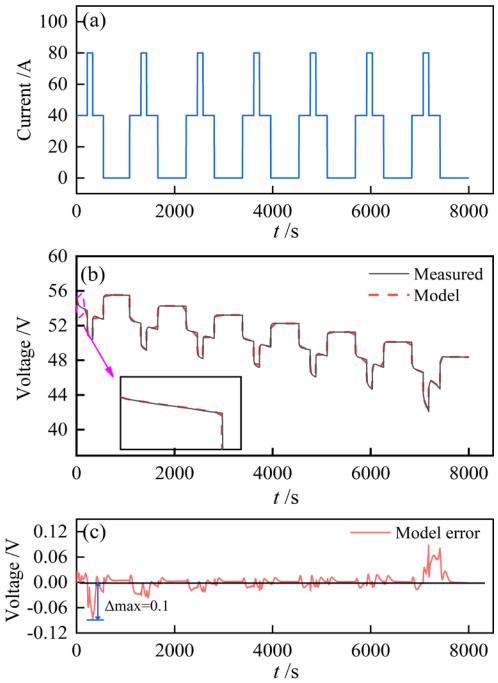

Fig. 4. Model validation. (a) Applied current. (b) Measured and simulated voltages. (c) Model error.

B. Experimental Design for Model Verification

To verify the developed VRB model, a hybrid pulse current discharge test was designed and used. The pulse current profile is shown in Fig. 4(a). Since the accuracy of the peak power estimation is affected by model parameters, the effectiveness of the online parameter identification algorithm is verified first. A similar approach described in [19] was used to identify other model parameters offline based on selected experimental data, while for the sake of brevity, this offline parameter identification procedure is not elaborated in the present work. Next, the measured battery voltage was compared with the model output in Fig. 4(b), and the model error is shown in Fig. 4(c). It can be seen that the predicted battery voltage is close to the experimental data: The maximum absolute error is less than 0.1 V, and the root-mean-square error (RMSE) of the model is 0.0165 V. These results show that the VRB model is suitable for the peak power estimation in the present study.

C. Experimental Design for Peak Power Estimation

Since the true peak power cannot be measured directly, it is calculated online based on the framework shown in Fig. 2. The results are benchmarked with the constant current/constant voltage pulses experiments [34]. In these experiments, the peak power is considered to be reached when either of the following two conditions is satisfied:

1) One of the cell voltages reaches or exceeds the SOA limits (i.e., $U_{t,\min}$ or $U_{t,\max}$) during the pulse while the current is within its predefined allowable region (i.e., $I_{\min} < I < I_{\max}$).

2) The current reaches or exceeds the SOA limits (i.e., $I_{\min}$ or $I_{\max}$) during the pulse while the cell voltages are all within their predefined allowable region (i.e., $U_{t,\min} < U_t < U_{t,\max}$).

Accordingly, five offline experiments for peak power verification were designed and carried out at SOC = 0.1, 0.3, 0.5, 0.7, and 0.9, respectively. Specifically, to test the discharge peak power at SOC = 0.1, the voltage of the VRB is controlled at the cut-off voltage $U_{t,\min}$. For calculating the discharge peak power at SOC = 0.3, the discharge current of the VRB is set to the minimum current $I_{\min}$. For the charge peak power at SOC = 0.5 and SOC = 0.7, the VRB is charged with the maximum current $I_{\max}$. Finally, for the charging peak power at SOC = 0.9, the voltage of the VRB is maintained at the maximum voltage $U_{t,\max}$.

In Fig. 5, two peak power estimation methods are compared with the proposed method. These are an RHC-UKF method with constant model parameters identified offline using the LS

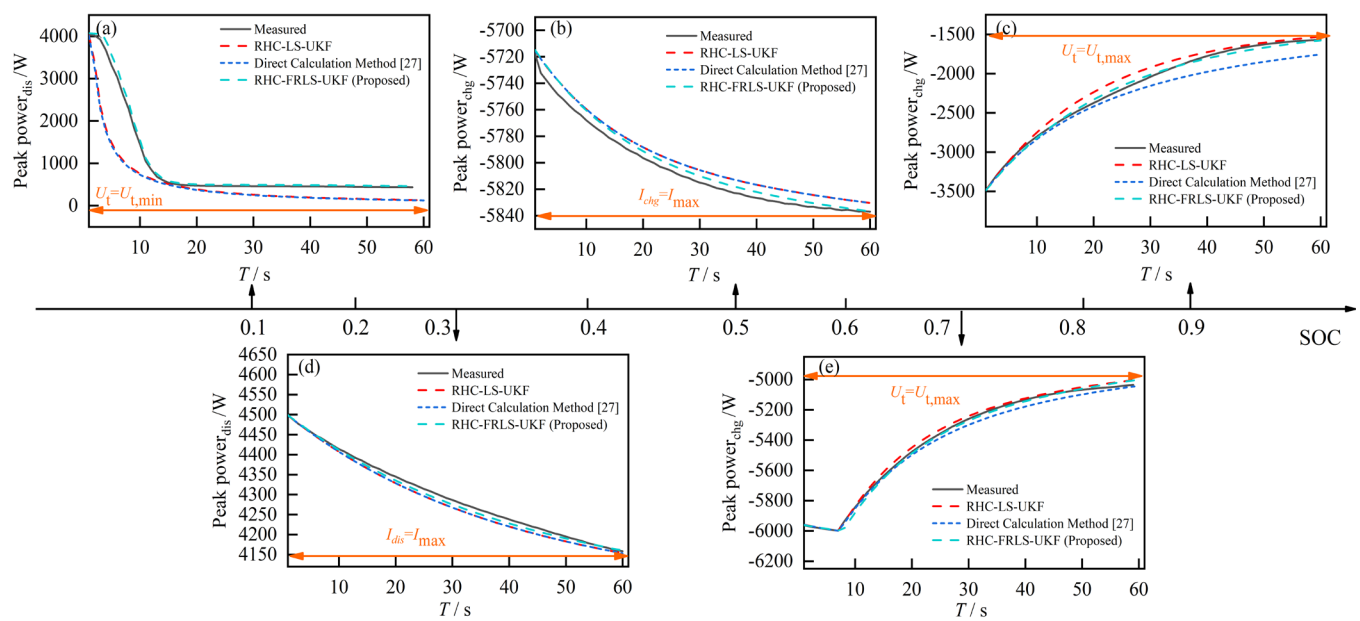

Fig. 5. Estimation results of VRB peak power for a time horizon of 60 s. (a) Discharging peak power constrained by the minimum voltage at SOC = 0.1. (b) Charging peak power constrained by the maximum current at SOC = 0.5. (c) Charging peak power constrained by the maximum voltage at SOC = 0.9. (d) Discharging peak power constrained by the maximum current at SOC = 0.3. (e) Charging peak power constrained by the maximum voltage at SOC = 0.7.

TABLE IV
COMPARISON OF RMSES WITH DIFFERENT VRB PEAK POWER ESTIMATION METHODS

	RHC-LS-UKF (Offline)	Direct Calculation Method [27]	RHC-FRLS-UKF (Proposed)
SOC = 0.9 (charge)	81.65 W	145.38 W	31.76 W
SOC = 0.7 (charge)	19.15 W	28.95 W	16.51 W
SOC = 0.5 (charge)	8.87 W	8.87 W	5.49 W
SOC = 0.3 (discharge)	13.91 W	13.91 W	7.71 W
SOC = 0.1 (discharge)	592.54 W	613.06 W	74.91W

method (denoted by RHC-LS-UKF) and the direct calculation method proposed in [27]. The prediction results of each method are benchmarked with the measurement data. The subfigures in Fig. 5 are lined up under SOCs of 0.1, 0.3, 0.5, 0.7, and 0.9, respectively. It can be observed from Fig. 5 that the results from the proposed method are close to the benchmark data. The results based on the proposed method show much smaller deviations from the measured data than the other two methods.

The main reason is that the proposed method has an online adjustment capability to follow the trends of battery terminal voltage, and the prediction with a moving horizon can update the battery operation states in time.

The accuracy of the proposed method is further analyzed and quantified by the RMSE of the peak power calculated under various SOCs. From Table IV, it can be seen that the proposed method has smaller RMSE compared to the other two methods. It is thus concluded that the proposed RHC-FRLS-UKF method exhibits high accuracy for VRB peak power estimation.

V. RESULTS AND DISCUSSION

A. VRB Model Validation

Obtaining accurate model parameters is important for peak power estimation. In this section, the measured current and voltage data from the hybrid pulse experiment were used to verify the FRLS-based online parameters identification. To initialize the parameter identification algorithm, the mean and covariance of the parameters need to be guessed. In this work, they are selected according to [20], i.e.,

$$\begin{cases} P_{\theta,0} = 10^6 \times I_4 \\ \theta_0 = \begin{bmatrix} 0.01 & 0.01 & 0.01 & 0.01 \end{bmatrix}^\top \end{cases}$$

The identified time-varying model parameters by the FRLS are plotted in Fig. 6. To verify the accuracy of results, we calculate the reference values of several selected points with a traditional offline method [19], indicated as the black dots in Fig. 6. It can be observed from Fig. 6 that the model parameters identified by FRLS are closed to the reference values. Thus, the VRB model with these online identified parameters can be considered accurate for peak power estimation.

B. UKF-Based VRB SOC Estimation

It is vital to accurately estimate the SOC since the peak power is affected by SOC. To evaluate the effectiveness of the UKF-based state estimator, in the hybrid pulse current discharge experiment, the initial SOC guess is set to 0.9 while the actual initial SOC is 0.96. The SOC estimation results and the corresponding estimation error are presented in Fig. 7(a) and Fig. 7(b), respectively. It shows that the estimated SOC rapidly

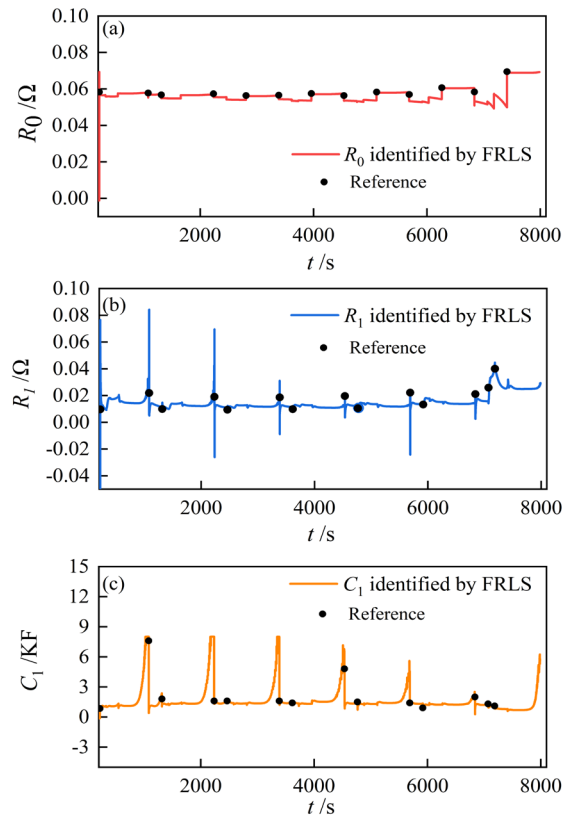

Fig. 6. Results of parameters identification: (a) R_0; (b) R_1; (c) C_1.

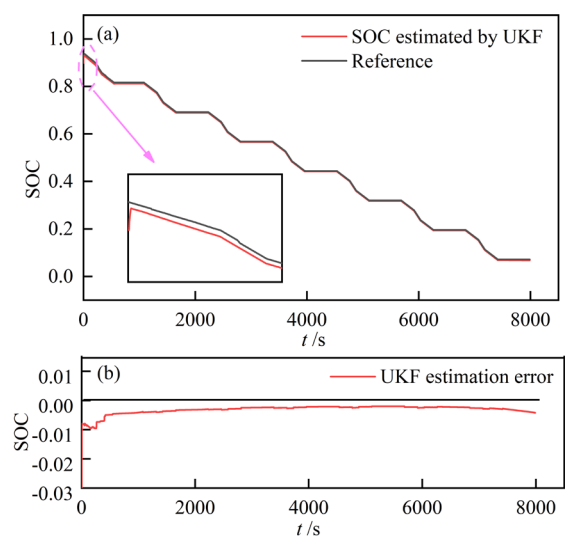

Fig. 7. Results of SOC estimation: (a) SOC. (b) Estimation error.

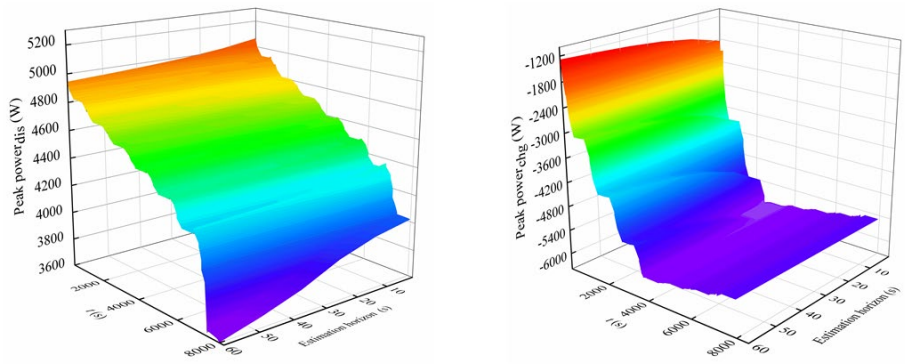

(a) (b)

Fig. 8. Peak power estimation under various prediction horizons. (a) Discharging peak power. (b) Charging peak power.

converges to the actual SOC within 100 s. Fig. 7(b) shows that the maximum absolute error is less than 0.03, and the RMSE is 0.01. Thus, the UKF-based VRB state estimator has achieved high accuracy for SOC estimation.

C. RHC-Based VRB Peak Power Estimation

Based on the identified model parameters and estimated states, the RHC-based peak power estimation is examined next under the current profile shown in Fig. 4(a). In Fig. 8, the predicted discharging and charging peak powers are plotted with various prediction horizons ranging from 10 s to 60 s. From Fig. 8(a), it can be observed that the discharge peak power drops as the battery SOC decreases. A significant peak power drop is observed at the end of the operating profile, and this is because, at the low SOC region, the active vanadium ions deplete rapidly, resulting in a drastic drop in the terminal voltage. It is noticed that the estimated peak power with a prediction horizon of 10 s is higher than that with a prediction horizon of 60 s, indicating that the continuous peak power capability of the VRB reduces as the stipulated time horizon increases. Compared to Fig. 8(a), as the battery SOC decreases, the magnitude of the charge peak power shown in Fig. 8(b) increases rapidly and then slightly decreases after about 4000 s. This phenomenon can be explained as follows: At the initial stage, the charge peak current is constrained by the maximum terminal voltage, and it rises due to the increasing difference between the voltage constraint and the OCV as the SOC decreases, leading to an increasing charging peak power when the VRB depletes. Nevertheless, after about 4000 s, the charging current can reach its maximum value, and the peak power drops due to the decreasing voltage.

The peak power capacity of VRBs with different prediction horizons is analyzed next. From Fig. 8, it is observed that both the estimated charging and discharging peak powers with a prediction horizon of 10 s are higher than those with a prediction horizon of 60 s. We plot a cross-section view of Fig. 8 with these two horizons in Fig. 9(a) to show the influence of the time horizon more clearly. Here, the shaded area enclosed by the nonlinear and unsymmetrical boundaries is the SOA of the VRB, which is subject to various factors, as mentioned earlier, such as the battery SOC, current and voltage limits, and

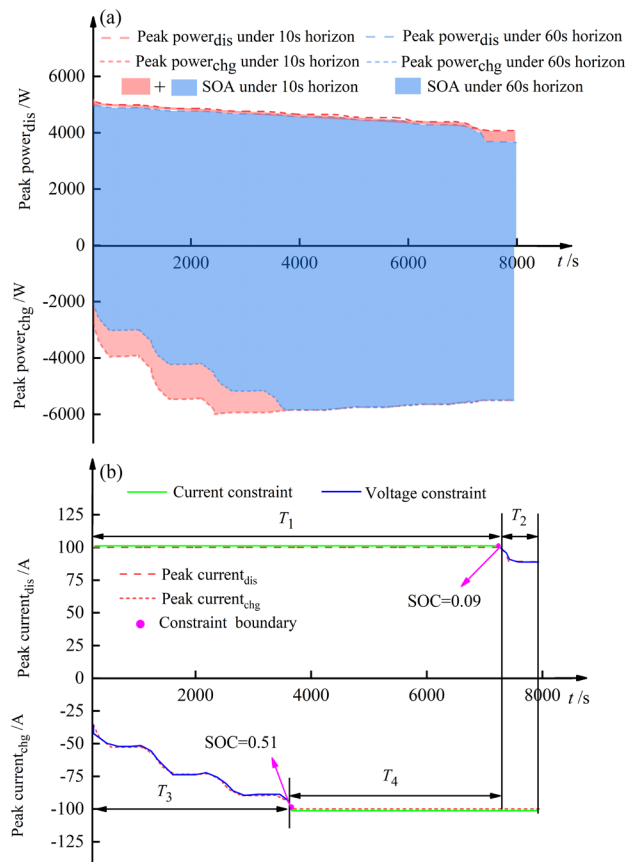

Fig. 9. A specific example under different prediction horizons. (a) Upper/lower limits and SOA under prediction horizon of 10 s and 60 s. (b) Battery constraints under prediction horizon of 60 s.

prediction horizon. To guarantee the safe operation of the VRB and to avoid overcharge/over-discharge, the operating point should not exceed the upper and lower limits (the dash boundaries as shown in the figure).

Furthermore, how the constraints limit the charging and discharging peak powers of VRBs at different charging or discharging stages are analyzed using Fig. 9(b). When the SOC and terminal voltage are high at the initial stage, the VRB does not reach its upper voltage limit even the maximum discharge current is applied. Thus, the active constraint at this stage (during the time interval T_1) is the maximum discharging

current, indicated by the upper green line, limiting the discharge peak power. This constraint is active until the SOC drops to 0.09, after which the terminal voltage will decrease significantly. At this stage (during the time interval T_2), the voltage constraint indicated by the upper blue curve affects the discharge peak power. On the other hand, for the charging peak power, the voltage constraint is the limiting factor during the time interval T_3 when the SOC > 0.51. When the SOC decreases and the terminal voltage drops, the maximum charging current limit of 100 A will be reached and play the limiting role during the time interval T_4.

Note that although $SOC_{min} = 0$ and $SOC_{max} = 1$ have been considered as the minimum and the maximum SOC levels in this example since the SOC range has been limited between 0.96 and 0.1 during the experiment, the SOC constraint did not come into effect.

VI. Conclusion

The peak power of vanadium redox flow batteries (VRBs) reflects the power delivery capacity of these energy storage systems in a short time interval. Accurate peak power estimation is thus essential for the safe, reliable, and efficient operation of VRBs. This paper proposed a receding horizon control (RHC) based peak power estimation method for VRBs. The paper proposes a novel RHC based peak power estimation algorithm to achieve high accuracy in predicting the peak power for VRB. The estimated peak power estimation algorithm is verified experimentally on a 5-kW/3-kWh VRB platform. The simulation and experimental results demonstrate the effectiveness of the proposed method.

References

[1] P. Zhao, H. Zhang, H. Zhou, J. Chen, S. Gao, and B. Yi, "Characteristics and performance of 10kW class all-vanadium redox-flow battery stack," *J. Power Sources*, vol. 162, no. 2, pp. 1416–1420, Nov. 2006.

[2] M. Skyllas-Kazacos, "Novel vanadium chloride/polyhalide redox flow battery," J. Power Sources, vol. 124, no. 1, pp. 299–302, Oct. 2003.

[3] A. Trovò, G. Marini, A. Sutto, P. Alotto, M. Giomo, F. Moro, and M. Guarnieri,A. Trovò et al., "Standby thermal model of a vanadium redox flow battery stack with crossover and shunt-current effects," *Appl. Energy*, vol. 240, pp. 893–906, Apr. 2019.

[4] Y. Li, J. Bao, M. Skyllas-Kazacos, M. P. Akter, X. Zhang, and J. Fletcher, "Studies on dynamic responses and impedance of the vanadium redox flow battery," *Appl. Energy*, vol. 237, pp. 91–102, Mar. 2019.

[5] R. Xiong, F. Sun, H. He, and T. D. Nguyen, "A data-driven adaptive state of charge and power capability joint estimator of lithium-ion polymer battery used in electric vehicles," *Energy*, vol. 63, pp. 295–308, Dec. 2013.

[6] X. Lai, L. He, S. Wang, L. Zhou, Y. Zhang, T. Sun, and Y. Zheng, "Co-estimation of state of charge and state of power for lithium-ion batteries based on fractional variable-order model," *J. Cleaner Prod*, vol. 255, p. 120203, May. 2020.

[7] F. Sun, R. Xiong, and H. He, "Estimation of state-of-charge and state-of-power capability of lithium-ion battery considering varying health conditions," *J. Power Sources*, vol. 259, pp. 166–176, Aug. 2014.

[8] W. Gan, X. Ai, J. Fang, M. Yan, and W. Yao, "Security constrained co-planning of transmission expansion and energy storage,"*Appl. Energy*, vol. 239, pp. 383–394, Apr. 2019.

[9] A. Farmann and D. U. Sauer, "A comprehensive review of on-board State-of-Available-Power prediction techniques for lithium-ion batteries in electric vehicles," *J. Power Sources*, vol. 329, pp. 123–137, Oct. 2016.

[10] F. Zheng, J. Jiang, B. Sun, W. Zhang, and M. Pecht, "Temperature dependent power capability estimation of lithium-ion batteries for hybrid electric vehicles," *Energy*, vol. 113, pp. 64–75, Oct. 2016.

[11] M. Sun, Y. Su, B. Xiong, H. Zhang, and Y. Li, "Online model identification method of vanadium redox flow battery based on time-varying forgetting factor recursive least squares," in *Proc. Chin. Autom. Congr. (CAC)*, Hangzhou, China, Nov. 2019.

[12] Y. Li, D. Karunathilake, D. M. Vilathgamuwa, Y. Mishra, T. W. Farrell, S. S. Choi, and C. Zou, "Model order reduction techniques for physics-based lithium-ion battery management: A survey," *IEEE Ind. Electron. Mag*, pp. 2–18, Aug. 2021.

[13] B. Xiong, J. Zhao, K. J. Tseng, M. Skyllas-Kazacos, T. M. Lim, and Y. Zhang, "Thermal hydraulic behavior and efficiency analysis of an all-vanadium redox flow battery," *J. Power Sources*, vol. 242, pp. 314–324, Nov. 2013.

[14] B. Jiang, H. Dai, X. Wei, and T. Xu, "Joint estimation of lithium-ion battery state of charge and capacity within an adaptive variable multi-timescale framework considering current measurement offset," *Appl. Energy*, vol. 253, p. 113619, Nov. 2019.

[15] X. Hu, F. Feng, K. Liu, L. Zhang, J. Xie, and B. Liu, "State estimation for advanced battery management: Key challenges and future trends," *Renew. Sustain. Energy Rev*, vol. 114, p. 109334, Oct. 2019.

[16] T. Weigert a, Q. Tianb, and K. Lianb "State-of-charge prediction of batteries and battery-supercapacitor hybrids using artificial neural networks," *J. Power Sources*, vol. 196, pp. 4061–4066, Feb. 2011.

[17] C. Burgos-Mellado, M. E. Orchard, M. Kazerani, R. Cárdenas, and D. Sáez, "Particle-filtering-based estimation of maximum available power state in Lithium-Ion batteries," *Appl. Energy*, vol. 161, pp. 349–363, Jan. 2016.

[18] J. Hu, H. Lin, X. Li, C. Jiang, X. Qiu, and W. Li, "State-of-charge estimation for battery management system using optimized support vector machine for regression," *J. Power Sources*, vol. 269, pp. 682–693, Dec. 2014.

[19] B. Xiong, J. Zhao, Y. Su, Z. Wei, and M. Skyllas-Kazacos, "State of charge estimation of vanadium redox flow battery based on sliding mode observer and dynamic model including capacity fading factor," *IEEE Trans. Sustain. Energy*, vol. 8, no. 4, pp. 1658–1667, Oct. 2017.

[20] Y. Qiu, X. Li, W. Chen, Z. Duan, and L. Yu, "State of charge estimation of vanadium redox battery based on improved extended Kalman filter," *ISA Trans.*, vol. 94, pp. 326–337, Nov. 2019.

[21] C. Zheng, X. Tian, G. Nie, Y. Yu, and Y. Li., "State of power and state of charge estimation of vanadium redox flow battery based on an online equivalent circuit model," in *Proc. IEEE 18th Int. Conf. Ind. Informat. (INDIN)*, Warwick, United Kingdom, Jul. 2020.

[22] X. Qiu, T. A. Nguyen, J. D. Guggenberger, M. L. Crow, and A. C. Elmore, "A field validated model of a vanadium redox flow battery for microgrids," *IEEE Trans. Smart Grid*, vol. 5, no. 4, pp. 1592–1601, Jul. 2014.

[23] Y. Zhang, J. Zhao, P. Wang, M. Skyllas-Kazacos, B. Xiong, and R. Badrinarayanan, "A comprehensive equivalent circuit model of all-vanadium redox flow battery for power system analysis," *J. Power Sources*, vol. 290, pp. 14–24, Sep. 2015.

[24] B. Xiong, Y. Yang, J. Tang, Y. Li, Z. Wei, Y. Su, and Q. Zhang., "An enhanced equivalent circuit model of vanadium redox flow battery energy storage systems considering thermal effects," *IEEE Access*, vol. 7, pp. 162297–162308, Nov. 2019.

[25] M. R. Mohamed, H. Ahmad, M. N. A. Seman, S. Razali, and M. S. Najib, "Electrical circuit model of a vanadium redox flow battery using extended Kalman filter," *J. Power Sources*, vol. 239, pp. 284–293, Oct. 2013.

[26] L. Yang, Y. Cai, Y. Yang, and Z. Deng, "Supervisory long-term prediction of state of available power for lithium-ion batteries in electric vehicles," *Appl. Energy*, vol. 257, p. 114006, Jan. 2020.

[27] Z. Wei, S. Meng, K. J. Tseng, T. M. Lim, B. H. Soong, and M. Skyllas-Kazacos, "An adaptive model for vanadium redox flow battery and its application for online peak power estimation," *J. Power Sources*, vol. 344, pp. 195–207, Mar. 2017.

[28] T. Feng, L. Yang, X. Zhao, H. Zhang, and J. Qiang, "Online identification of lithium-ion battery parameters based on an improved equivalent-circuit model and its implementation on battery state-of-power prediction," J. *Power Sources*, vol. 281, pp. 192–203, May. 2015.

[29] C. Zou, A. Klintberg, Z. Wei, B. Fridholm, T. Wik, and B. Egardt, "Power capability prediction for lithium-ion batteries using economic nonlinear model predictive control," *J. Power Sources*, vol. 396, pp. 580–589, Aug. 2018.

[30] G. Dong, J. Wei, and Z. Chen, "Kalman filter for onboard state of charge estimation and peak power capability analysis of lithium-ion batteries," *J. Power Sources*, vol. 328, pp. 615–626, Oct. 2016.

[31] W. Zhang, W. Shi, and Z. Ma, "Adaptive unscented Kalman filter based state of energy and power capability estimation approach for lithium-ion battery," *J. Power Sources*, vol. 289, pp. 50–62, Sep. 2015.

[32] Y. Li, Z. Wei, B. Xiong, and D. M. Vilathgamuwa, "Adaptive ensemble-based electrochemical-thermal-degradation state estimation of lithium-ion batteries," *IEEE Trans. Ind. Electron*, early access, Jul. 2021.
[33] S. Li, K. Li, E. Xiao, J. Zhang, and M. Zheng, "Real-time peak power prediction for zinc nickel single flow batteries," *J. Power Sources*, vol. 448, p. 227346, Feb. 2020.
[34] M. J. Esfandyari, M. R. Hairi Yazdi, V. Esfahanian, M. Masih-Tehrani, H. Nehzati, and O. Shekoofa, "A hybrid model predictive and fuzzy logic based control method for state of power estimation of series-connected Lithium-ion batteries in HEVs," *J. Energy Storage*, vol. 24, p. 100758, Aug. 2019.

Binyu Xiong (Member, IEEE) received the B.E. degree in electrical engineering from Wuhan University, Wuhan, China, in 2010, and the MSc. and the Ph.D. degrees from Nanyang Technological University, Singapore in 2011 and 2016, respectively, both in power engineering. He is currently an Associate Professor with the School of Automation, Wuhan University of Technology, Wuhan. His research interests include battery modeling, state of charge estimation, large-scale energy storage systems, power electronics, and renewable energy generations.

Sidi Dong received the B.E. degree in electrical engineering

Yang Li (Member, IEEE) received the B.E. degree in electrical engineering from Wuhan University, Wuhan, China, in 2007, and the M.Sc. and Ph.D. degrees in power engineering from Nanyang Technological University (NTU), Singapore, in 2008 and 2015, respectively.
From 2015 to 2018, he was a Research Fellow with the Energy Research Institute, NTU, and the School of Electrical Engineering and Computer Science, Queensland University of Technology, Brisbane, QLD, Australia. Since 2019, he has been an Associate Professor with the School of Automation, Wuhan University of Technology, Wuhan. He is currently a Researcher with the Department of Electrical Engineering, Chalmers University of Technology, Gothenburg, Sweden. His research interests include modeling and control of energy storage systems in power systems and transport sector.

Jinrui Tang (Member, IEEE) received the B.S. degree in electrical engineering from Zhejiang University, Hangzhou, China, in 2009, and the Ph.D. degree in electrical engineering from the School of Electrical and Electronics Engineering, Huazhong University of Science and Technology, Wuhan, China, in 2014. He is currently an Associate Professor with the School of Automation, Wuhan University of Technology, Wuhan. His research interests include power system protection.

Zhongbao Wei (Senior Member, IEEE) received the B.Eng. and M.Sc. degrees in instrumental science and technology from Beihang University. Beijing, China, in 2010 and 2013, respectively, and the Ph.D. degree in power engineering from Nanyang Technological University (NTU), Singapore, in 2017. He was a Research Fellow with the Energy Research Institute at NTU from 2016 to 2018. He is currently a Professor in vehicle engineering with the National Engineering Laboratory for Electric Vehicles, Beijing Institute of Technology, Beijing. He has authored more than 70 peer-reviewed articles.

Yixin Su received the B.E. degree in electrical engineering